

Spin relaxation in a GaAs quantum dot embedded inside a suspended phonon cavity

Y. Y. Liao,¹ Y. N. Chen,¹ D. S. Chuu,^{1,*} and T. Brandes²

¹*Department of Electrophysics, National Chiao-Tung University, Hsinchu 300, Taiwan*

²*School of Physics and Astronomy, The University of Manchester P.O. Box 88, Manchester, M60 1QD, U.K.*

(Dated: January 30, 2019)

The phonon-induced spin relaxation in a two-dimensional quantum dot embedded inside a semiconductor slab is investigated theoretically. An enhanced relaxation rate is found due to the phonon van Hove singularities. Oppositely, a vanishing deformation potential may also result in a suppression of the spin relaxation rate. For larger quantum dots, the interplay between the spin orbit interaction and Zeeman levels causes the suppression of the relaxation at several points. Furthermore, a crossover from confined to bulk-like systems is obtained by varying the width of the slab.

PACS numbers: 73.21.La, 71.70.Ej, 63.20.Dj, 72.25.Rb

Spin properties in nanostructures have become a field of intense research ranging from spin field-effect transistor,¹ spin-polarized p-n junctions² up to quantum spin computers.³ The quantum dot (QD) may be a good choice for quantum electronics due to its zero dimensionality, quantized energy levels, and long coherence times of spin states.^{6,7} For example, the spin of an electron confined to a QD can form a qubit.^{4,5} However, some scattering processes will cause the change of the spin states. One important process is related to the phonon-induced spin-flip resulting from the spin-orbit interaction. This affects the time of spin purity in the QD. In order to keep the information unchanged, a long relaxation time is required.

In general, the spin-orbit (SO) coupling, which is one of the main causes of spin relaxation, is a relevant intrinsic interaction in nonmagnetic semiconductors. It is known that there are two different types of spin-orbit coupling as QDs are fabricated within semiconductors of a zincblende structure. The first one is the Dresselhaus interaction, which is due to the bulk inversion asymmetry of the lattice.^{8,9,10} The second is the Rashba interaction caused by the structure inversion asymmetry.¹¹ The spin-orbit couplings mix the spin states with different orientations in the Zeeman sublevels^{12,13,14,15} and therefore make spin relaxation possible in the presence of the electron-phonon interaction.

Relaxation times of electron spins in a QD have been measured by electrical pump-probe experiments.¹⁶ The triplet-to-singlet transition with emission of phonons was found with corresponding spin relaxation times of about 200 μ s. Recently, the spin relaxation time in a one-electron GaAs QD was measured by a similar electrical pump-probe technique.^{17,18} As the magnetic field was applied parallel to the two-dimensional electron gas, the Zeeman splitting of QD was observed in dc transport spectroscopy. By monitoring the relaxation of the spin, the relaxation time was found to have a lower bound of 50 μ s at an in-plane field of 7.5 T.¹⁷

On the theoretical side, spin relaxation between two spin-mixed states in semiconductor QDs has been studied recently. However, to the best of our knowledge, all previous studies of spin relaxation have concentrated

on QDs embedded in the bulk material,^{19,20,21,22,23,24} whereas studies of spin relaxation induced by confined phonons are still lacking. In this work, we therefore consider a single QD embedded into a free-standing structure (semiconductor slab), where the relevant characteristic is the two-dimensional phonon wavevector for the acoustic-phonon spectrum as shown in Fig. 1.^{25,26,27,28,29} Since the reduced dimension will enhance the deformation potential, we will mainly focus on the spin relaxation rate induced by the deformation potential.^{25,26,27} In this paper we describe the model with spin-orbit coupling. Energy spectra of the QD can be solved by using an exact diagonalization method. We then apply the Fermi golden rule to calculate spin relaxation rates for typical parameters. We discuss the dependence of the spin relaxation rates on the size of the QD, the phonon bath temperature, and the width of the slab.

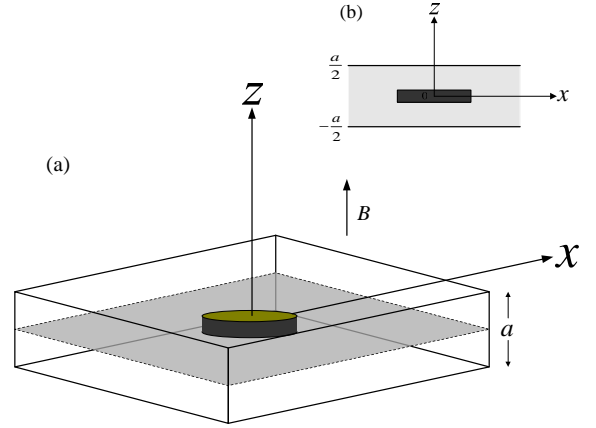


FIG. 1: (Color online) (a) Schematic view of single QD embedded in the semiconductor slab with a width of a . (b) The side view shows a QD is located at $z = 0$.

We consider an isotropic QD with an in-plane parabolic lateral confinement potential. An external magnetic field B is applied perpendicularly to the surface of the QD as shown in Fig. 1(a). The electronic Hamiltonian of this system can be written as

$$H_e = H_0 + H_{so}. \quad (1)$$

The first term describes the electron Hamiltonian without the spin-orbit coupling,

$$H_0 = \frac{\mathbf{P}^2}{2m^*} + \frac{1}{2}m^*\omega_0^2r^2 + \frac{1}{2}g^*\mu_B B\sigma_z, \quad (2)$$

where $\mathbf{P} = -i\hbar\nabla + (e/c)\mathbf{A}$ is the kinetic momentum with vector potential $\mathbf{A} = (B/2)(-y, x, 0)$ confined to the 2D plane. Here m^* is the effective electron mass, e is the electron charge, c is the velocity of light, ω_0 is the characteristic confined frequency, g^* is the bulk g -factor, μ_B is the Bohr magneton, and σ_z is a Pauli matrix.

The Rashba and Dresselhaus interactions ($H_{so} = H_R + H_D$) are given by

$$H_R = \frac{\lambda_R}{\hbar}(\sigma_x P_y - \sigma_y P_x), \quad (3)$$

$$H_D = \frac{\lambda_D}{\hbar}(-\sigma_x P_x + \sigma_y P_y). \quad (4)$$

The coupling constants λ_R and λ_D determine the spin-orbit strengths, which depend on the band-structure parameters of the material. Besides, the Rashba and Dresselhaus terms are also associated to the perpendicular confinement field and the confinement width in the z -direction, respectively.

For the electron Hamiltonian H_0 , the well-known Fock-Darwin states $\Psi_{n,l,\sigma}$ can be easily obtained. The corresponding electron energy levels are $E_{n,l,\sigma} = \hbar\Omega(2n + |l| + 1) + \hbar\omega_B l/2 + \sigma E_B$, where n ($= 0, 1, 2, \dots$) and l ($= 0, \pm 1, \pm 2, \dots$) are the quantum numbers. The renormalized frequency is $\Omega = \sqrt{\omega_0^2 + \omega_B^2}$, with the cyclotron frequency $\omega_B = eB/m^*$ and the characteristic confinement frequency ω_0 limited by the effective QD lateral length $l_0 = \sqrt{\hbar/m^*\omega_0}$. Here, $E_B = g\mu_B B/2$ is the Zeeman splitting energy, and $\sigma = \pm 1$ refers to the electron-spin polarization along the z axis. To solve the Schrödinger equation with ($H_e = H_0 + H_{so}$), the (spin mixing) wave function is expressed in terms of a series of eigenfunctions: $\Psi_\ell(r, \theta) = \sum c_{n,l,\sigma} \Psi_{n,l,\sigma}$ for each state ℓ . After exactly diagonalizing the electron Hamiltonian, the corresponding eigenvalues E_ℓ and the coefficient $c_{n,l,\sigma}$ can be obtained numerically.

Before calculating the spin relaxation rate, the confined phonon in the free-standing structure must be introduced here. Following Re. [25], we consider an infinite film with width a (Fig. 1). For the effect of the contact with the semiconductor substrate, we neglect the distortion of the acoustic vibrations. Under this consideration, one can ensure that the in-plane wavelength can be shorter than the characteristic in-plane size of the solid slab. For simplicity, the elastic properties of the slab are isotropic. Small elastic vibrations of a solid slab can then be defined by a vector of relative displacement $\mathbf{u}(\mathbf{r}, t)$. Under the isotropic elastic continuum approximation, the displacement field \mathbf{u} obeys the equation

$$\frac{\partial^2 \mathbf{u}}{\partial t^2} = c_t^2 \nabla^2 \mathbf{u} + (c_l^2 - c_t^2) \nabla (\nabla \cdot \mathbf{u}), \quad (5)$$

where c_l and c_t are the velocities of longitudinal and transverse bulk acoustic waves. To define a system of confined modes, Eq. (5) should be complemented by the boundary conditions at the slab surface $z = \pm a/2$. Because of the confinement, phonons will be quantized in subbands. For each in-plane component \mathbf{q}_\parallel of the in-plane wave vector there are infinitely many subbands. Since two types of velocities of sound exist in the elastic medium, there are also two transversal wavevectors q_l and q_t . In the following, we consider the deformation potential only. This means there are two confined acoustic modes: dilatational waves and flexural waves contribute, but shear waves are neglected because of their vanishing interaction with the electrons for spin relaxation.

For dilatational waves, the parameters $q_{l,n}$ and $q_{t,n}$ can be determined from the Rayleigh-Lamb equation

$$\frac{\tan(q_{t,n}a/2)}{\tan(q_{l,n}a/2)} = -\frac{4q_\parallel q_{l,n} q_{t,n}}{(q_\parallel^2 - q_{t,n}^2)^2}, \quad (6)$$

with the dispersion relation

$$\omega_{n,q_\parallel} = c_l^2 \sqrt{q_\parallel^2 + q_{l,n}^2} = c_t^2 \sqrt{q_\parallel^2 + q_{t,n}^2}, \quad (7)$$

where ω_{n,q_\parallel} is the frequency of the dilatational wave in mode $(n, \mathbf{q}_\parallel)$. For the antisymmetric flexural waves, the solutions $q_{l,n}$ and $q_{t,n}$ also can be determined by solving the equation

$$\frac{\tan(q_{l,n}a/2)}{\tan(q_{t,n}a/2)} = -\frac{4q_\parallel q_{l,n} q_{t,n}}{(q_\parallel^2 - q_{t,n}^2)^2}, \quad (8)$$

together with the dispersion relation, Eq. (7).

The electron-phonon interaction through the deformation is given by $H_{ep} = E_a \text{div} \mathbf{u}$, where E_a is the deformation-potential coupling constant. The Hamiltonian can be written as

$$H_{ep} = \sum_{\substack{\mathbf{q}_\parallel, n \\ \lambda=d,f}} M_\lambda(\mathbf{q}_\parallel, n, z)(a_{\mathbf{q}_\parallel}^+ + a_{\mathbf{q}_\parallel}) \exp(i\mathbf{q}_\parallel \cdot \mathbf{r}_\parallel), \quad (9)$$

where \mathbf{r}_\parallel is the coordinate vector in the x - y plane and the functions M_d and M_f describe the intensity of the electron interactions with the dilatational and flexural waves, and are given by

$$M_d(q_\parallel, n, z) = F_{d,n} \sqrt{\frac{\hbar E_a^2}{2A\rho\omega_{n,q_\parallel}}} \times \left[(q_{t,n}^2 - q_\parallel^2)(q_{t,n}^2 + q_\parallel^2) \times \sin\left(\frac{aq_{t,n}}{2}\right) \cos(q_{l,n}z) \right], \quad (10)$$

$$M_f(q_\parallel, n, z) = F_{f,n} \sqrt{\frac{\hbar E_a^2}{2A\rho\omega_{n,q_\parallel}}} \times \left[(q_{t,n}^2 - q_\parallel^2)(q_{t,n}^2 + q_\parallel^2) \times \cos\left(\frac{aq_{t,n}}{2}\right) \sin(q_{l,n}z) \right], \quad (11)$$

where A is the area of the slab, ρ is the mass density, and $F_{d,n}$ ($F_{f,n}$) is the the normalization constants of the n -th eigenmode for the dilatational (flexural) waves. Although the fluctuation of the dot (due to strain etc.) may affect the spin-orbit and electron-phonon coupling, we, for simplicity, neglect the effect on the scattering rate in this work.

We calculate the spin relaxation rates between the two lowest (spin mixing) states from the Fermi golden rule³⁰

$$\Gamma = \frac{2\pi}{\hbar} \sum_{\substack{\mathbf{q}_{\parallel}; n \\ \lambda=d,f}} |M_{\lambda}|^2 |\langle f | e^{i\mathbf{q}_{\parallel} \cdot \mathbf{r}_{\parallel}} | i \rangle|^2 \times (N_{q_{\parallel}} + 1) \delta(\Delta E - \hbar\omega_{n,q_{\parallel}}), \quad (12)$$

where the energy ΔE ($= E_i - E_f$) is the energy difference between the first excited $|i\rangle$ and ground $|f\rangle$ states. $N_{q_{\parallel}}$ represents the Bose distribution of the phonon at temperature T . For the sake of simplicity, we consider the QD to be located at $z = 0$ so that the function M_f for flexural waves plays no role.

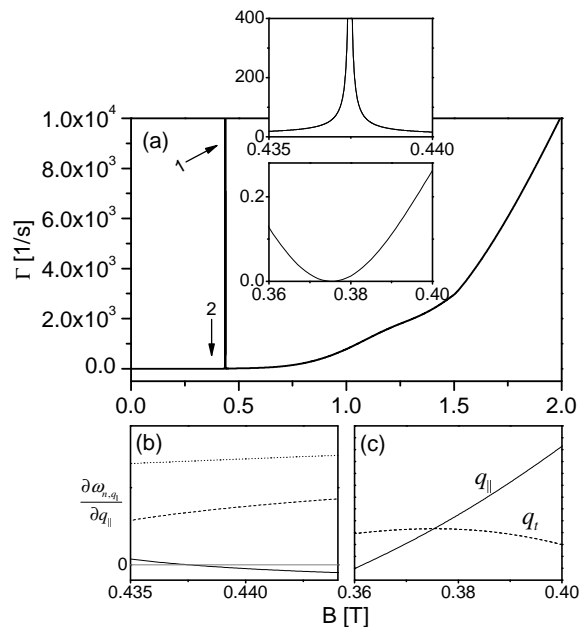


FIG. 2: (a) Spin relaxation rate as a function of magnetic field for the lateral length $l_0 = 30$ nm, the width $a = 130$ nm, and temperature $T=100$ mK. The SO couplings λ_R and λ_D are set equal to 5×10^{-13} and 16×10^{-12} eV m, respectively. The insets further show the enlarged regions of arrow 1 (upper inset) and arrow 2 (lower inset). (b) Three phonon group velocities vs the magnetic field. (c) The values q_{\parallel} and q_t vs the magnetic field.

Let us first focus on the dependence of the relaxation rates on the magnetic field B for lateral length $l_0 = 30$ nm. Unlike the situation in bulk system, an enhanced spin relaxation rate occurs as shown in Fig. 2(a) (arrow 1 in the upper inset). This phenomenon originates from the van Hove singularity that corresponds to a minimum in the dispersion relation $\omega_{n,q_{\parallel}}$ for finite q_{\parallel} . We further

plot the phonon group velocity ($\partial\omega_{n,q_{\parallel}}/\partial q_{\parallel}$) as a function of q_{\parallel} around the van Hove singularity as shown in Fig. 2(b). There are three modes contributing to the relaxation rate. In particular, a crossover from positive to negative group velocity is observed for one mode. Because of the zero phonon group velocity, the rate behaves sharply at that magnetic field. However in a real system the van Hove singularity would be cut off or broadened because of the finite phonon lifetime. Contrary to the enhanced rate, we find a suppression of the spin relaxation rate (arrow 2) at small magnetic field (also seen in the lower inset). This comes from a vanishing divergence of the displacement field \mathbf{u} . As can be seen from Eq. (10) in detail, the deformation potential disappears at the condition of $q_{\parallel} = q_t$ (Fig. 2(c)), which causes a zero spin relaxation rate. Note that our results for the van Hove singularity and the disappearance of the deformation potential are consistent with what was found in Ref. [27]. Although the phonon model in our work is the same, the dot part is different.

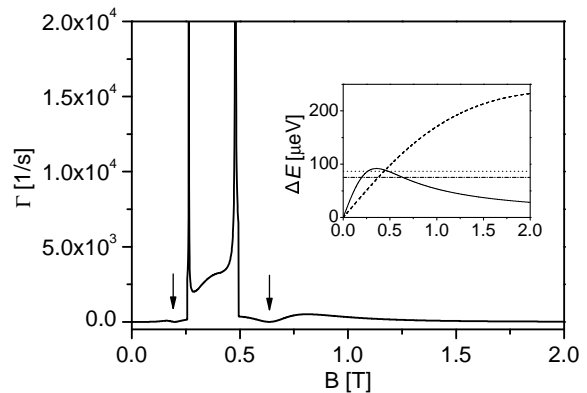


FIG. 3: Spin relaxation rate for the lateral length $l_0 = 60$ nm, width $a = 130$ nm, and temperature $T=100$ mK. The SO couplings λ_R and λ_D are set equal to 5×10^{-13} and 16×10^{-12} eV m, respectively. Two enhanced and suppressed rates (arrow) occur. The inset shows the energy spacing ΔE vs the magnetic field B for different lateral lengths: $l_0 = 30$ nm (dashed line) and $l_0 = 60$ nm (solid line). Two horizontal lines in the inset indicate the corresponding energies for the van Hove singularity (dotted line) and the suppression of the rate (dashed-dotted line).

The relaxation rate for larger QDs exhibits a qualitatively different behavior. As shown in Fig. 3, two van Hove singularities appear when varying the magnetic field. Besides, one also finds two suppressions of the relaxation rate (arrow) near the singularities. We have analyzed the energy spacing between the two lowest states in the inset of Fig. 3. For small lateral size, the gap increases monotonically (dashed line). On the contrary, energy spacing for larger QDs shows a quite different feature. The value initially increases as B increases. However, after it reaches a maximum point, the energy spacing decreases with the increasing of the magnetic field B : although the Zeeman splitting increases with increasing

magnetic field, the spin-orbit interaction, on the contrary, tends to reduce the energy spacing between the two lowest levels. When the magnetic field is large enough, the spin-orbit effect overwhelms the Zeeman term and results in a decreasing tendency. Therefore, if the magnetic field is increased high enough, the dashed line (small QD) also shows similar behavior. This agrees well with the findings in Ref. [14]. From the inset, one recognizes that if the energy spacing exactly matches the specific phonon energy (dotted line), the van Hove singularity will appear. For the case of a large lateral length, there are two van Hove singularities and two suppressions of the relaxation rate (dashed-dotted line).

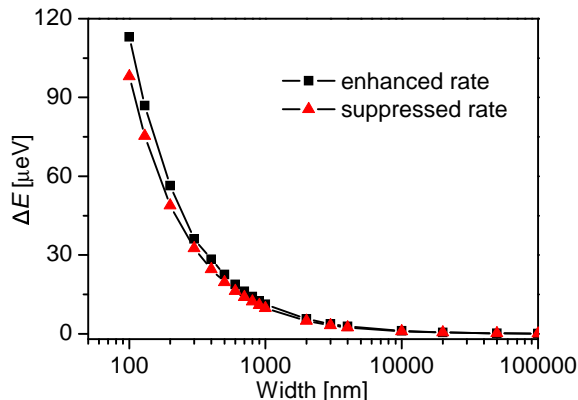


FIG. 4: (Color online) Dependence of the specific energy spacings ΔE for the enhanced (black mark) and suppressed (red mark) rates on the width a . The lateral length of the QD is 30 nm. The Rashba constant is $\lambda_R = 5 \times 10^{-12}$ eVm and the Dresselhaus constant is $\lambda_D = 16 \times 10^{-12}$ eVm.

Fig. 4 shows the specific energy spacings where rates are enhanced and suppressed as a function of the width. For the case of small widths, the enhanced rates (black mark) and suppressed rates (red mark) can be clearly distinguished, and their corresponding energy spacings are relative large. With the increasing of the width, the energy spacing between the enhanced and suppressed rates decrease monotonically. One can expect that if the width increases further, the system will approach the bulk system. This means that the van Hove singularity and the

suppressed rate will be inhibited and eventually disappear.

If one varies the vertical position of the dot, the rate will change due to different contributions from the dilatational and flexural waves. Accordingly, the van Hove singularities resulting from flexural waves will also be altered. For example, the ratio of dilatational to flexural wave's contribution is about 2.8:1 under the condition of $B = 1$ T and vertical position $z = 25$ nm. However, if ΔE also changes, the contributions from two waves will also change. This is because the parameters ($q_{\parallel}, q_{l,n}, q_{t,n}$) of dilatational and flexural waves independently satisfy the dispersion relations. On the other hand, comparing the bulk phonons with the confined ones, the phonon-induced rates are roughly similar when varying the magnetic field. However, there are two peculiar characteristics for the confined phonons. One feature is the van Hove singularity which results from a zero group velocity such that an enhanced spin relaxation rate can occur. The second feature is a vanishing divergence of the displacement field. This will cause a suppression of spin relaxation rate, which is an advantage if considering the QD spin as a possible quantum bit candidate.

We have studied the spin relaxation rate in a GaAs quantum dot embedded in a semiconductor slab, where an enhanced rate was found due to the phonon van Hove singularity. We found that at certain magnetic fields one enters a regime with quite the opposite characteristics, where a vanishing divergence of the displacement causes a suppression of spin relaxation rates. For larger dots there are multiple singularities and suppressions in the electron-phonon rates due to the interplay between spin-orbit coupling and Zeeman interaction. We believe our results to be useful for the understanding of spin relaxation in suspended quantum dot nanostructures. Our findings also point at novel effects to be expected from future nano-scale systems where spin and mechanical degrees of freedom are combined.

This work is supported partially by the National Science Council, Taiwan under the grant numbers NSC 94-2112-M-009-019, NSC 94-2120-M-009-002 and NSC 94-2112-M-009-024.

* Corresponding author; Electronic address: dschuu@mail.nctu.edu.tw

¹ S. Datta and B. Das, Appl. Phys. Lett. **56**, 665 (1990).

² I. Žutić, J. Fabian, and S. Das Sarma, Phys. Rev. Lett. **88**, 066603 (2002).

³ D. Loss and D. P. DiVincenzo, Phys. Rev. A **57**, 120 (1998); G. Burkard, D. Loss, and D. P. DiVincenzo, Phys. Rev. B **59**, 2070 (1999).

⁴ X. Hu and S. Das Sarma, Phys. Rev. A **61**, 062301 (2000).

⁵ M. Friesen, P. Rugheimer, D. E. Savage, M. G. Lagally, D. W. van der Weide, R. Joynt, and M. A. Eriksson, Phys.

Rev. B **67**, 121301(R) (2003).

⁶ S. M. Reimann and M. Manninen, Rev. Mod. Phys. **74**, 1283 (2002).

⁷ W. G. van der Wiel, S. De Franceschi, J. M. Elzerman, T. Fujisawa, S. Tarucha, and L. P. Kouwenhoven, Rev. Mod. Phys. **75**, 1 (2003).

⁸ G. Dresselhaus, Phys. Rev. **100**, 580 (1955).

⁹ M. I. D'yakonov and V. I. Perel', Zh. Éksp. Teor. Fiz. **60**, 1954 (1971) [Sov. Phys. JETP **38**, 1053 (1971)].

¹⁰ M. I. D'yakonov and V. Yu. Kachorovskii, Fiz. Tekh. Poluprovodn. **20**, 178 (1986) [Sov. Phys. Semicond. **20**,

- 110 (1986)].
- ¹¹ Yu. L. Bychkov and E. I. Rashba, JETP Lett. **39**, 78 (1984); J. Phys. C **17**,6039 (1984).
 - ¹² O. Voskoboynikov, C. P. Lee, and O. Tretyak, Phys. Rev. B **63**, 165306 (2001).
 - ¹³ C. F. Destefani, S. E. Ulloa, and G. E. Marques, Phys. Rev. B **70**, 205315 (2004).
 - ¹⁴ C. F. Destefani and S. E. Ulloa, Phys. Rev. B **71**, 161303(R) (2005).
 - ¹⁵ S. Debal and C. Emary, Phys. Rev. Lett. **94**, 226803 (2005).
 - ¹⁶ T. Fujisawa, D. G. Austing, Y. Tokura, Y. Hirayama, and S. Tarucha, Nature (London) **419**, 278 (2002).
 - ¹⁷ R. Hanson, B. Witkamp, L. M. K. Vandersypen, L. H. Willems van Beveren, J. M. Elzerman, and L. P. Kouwenhoven, Phys. Rev. Lett. **91**, 196802 (2003).
 - ¹⁸ J. M. Elzerman, R. Hanson, L. H. Willems van Beveren, B. Witkamp, L. M. K. Vandersypen, and L. P. Kouwenhoven, Nature (London) **430**, 431 (2004).
 - ¹⁹ A. V. Khaetskii and Y. V. Nazarov, Phys. Rev. B **61**, 12639 (2000); **64**, 125316 (2001).
 - ²⁰ L. M. Woods, T. L. Reinecke, and Y. Lyanda-Geller, Phys. Rev. B **66**, 161318(R) (2002).
 - ²¹ R. de Sousa and S. Das Sarma, Phys. Rev. B **68**, 155330 (2003).
 - ²² V. N. Golovach, A. Khaetskii, and D. Loss, Phys. Rev. Lett. **93**, 016601 (2004).
 - ²³ J. L. Cheng, M. W. Wu, and C. Lü, Phys. Rev. B **69**, 115318 (2004).
 - ²⁴ D. V. Bulaev and D. Loss, Phys. Rev. B **71**, 205324 (2005).
 - ²⁵ N. Bannov, V. Aristov, V. Mitin, and M. A. Stroschio, Phys. Rev. B **51**, 9930 (1995); N. Bannov, V. Mitin and M. A. Stroschio, Phys. Status Solidi B **183**, 131 (1994).
 - ²⁶ B. A. Glavin, V. I. Pipa, V. V. Mitin, and M. A. Stroschio, Phys. Rev. B **65**, 205315 (2002).
 - ²⁷ S. Debal, T. Brandes, and B. Kramer, Phys. Rev. B **66**, 041301(R) (2002).
 - ²⁸ E. M. Höhberger, T. Krämer, W. Wegscheider, and R. H. Blick, Appl. Phys. Lett. **82**, 4160 (2003).
 - ²⁹ E. M. Weig, R. H. Blick, T. Brandes, J. Kirschbaum, W. Wegscheider, M. Bichler, and J. P. Kotthaus, Phys. Rev. Lett. **92**, 046804 (2004).
 - ³⁰ The parameters for the GaAs QD: $m = 0.067 m_0$, $g^* = -0.44$, $E_a = 6.7$ eV, $\rho = 5.3 \times 10^3$ Kg/m³, $c_t = 3.35 \times 10^3$ m/s, $c_l = 5.7 \times 10^3$ m/s.